Numerical Heat Transfer, Part A, 42: 465–486, 2002

1040-7782/02 $12.00 + .00
DOI: 10.1080/10407780290059657

DOUBLE-DIFFUSIVE MIXED CONVECTION IN A LID-DRIVEN ENCLOSURE FILLED WITH A FLUID-SATURATED POROUS MEDIUM

K. Khanafer
Department of Mechanical Engineering, The Ohio State University, Columbus, Ohio, USA

K. Vafai
Department of Mechanical Engineering, University of California, Riverside, California, USA

This article presents a numerical study of mixed-convection heat and mass transport in a lid-driven square enclosure filled with a non-Darcian fluid-saturated porous medium. The two vertical walls of the enclosure are insulated, while the horizontal walls are kept at constant but different temperatures and concentrations with the top surface moving at a constant speed. The transport equations are solved numerically using the finite-volume approach along with the alternating direct implicit (ADI) procedure. Comparisons with previously published work are performed and found to be in excellent agreement. The results of the present investigation indicate that the buoyancy ratio, Darcy number, Lewis number, and Richardson number have profound effects on the double-diffusive phenomenon.

INTRODUCTION

Double-diffusive convection or thermosolutal convection is generally referred to fluid flows generated by buoyancy effects due to both temperature and concentration gradients. This type of flow is encountered in natural and technological applications. Such applications include the growth of crystals, solar energy systems, welding processes, thermal insulations, etc. [1–5]. Most of the analytical and numerical studies presented in the literature are based on the combined heat and mass transfer natural convection in enclosures with fixed walls. A comprehensive review of the natural convection due to combined thermal and solutal driving forces was conducted by Ostrach [6]. Ranganathan and Viskanta [7] investigated both analytically and numerically natural convection in a two-dimensional square cavity filled with a binary gas due to combined temperature and concentration gradients. The analysis indicated that the velocities at the vertical walls were inversely proportional to the concentration parameter. Trevisan and Bejan [8] investigated numerically and

Received 17 December 2001; accepted 15 February 2002.
Address correspondence to Kambiz Vafai, University of California, Riverside, Department of Mechanical Engineering, A363 Bourns Hall, Riverside, CA 92521-0425, USA. E-mail: vafai@engr.ucr.edu

NOMENCLATURE

A	aspect ratio, $(=L/H)$
Bi_c	solutal Biot number $(=h_c H/D)$
c	specific heat at constant pressure
C'	concentration
C	normalized concentration $[=(C'-C'_C)/(C'_H-C'_C)]$
D	diffusion coefficient
Da	Darcy number $(=K/H^2)$
F	geometric function
$\mathbf{g}$	gravitational acceleration vector
Gr_C	solutal Grashof number $(=g\beta_C \Delta C' H^3/\nu^2)$
Gr_T	Grashof number $(=g\beta_T \Delta T H^3/\nu^2)$
H	cavity height
h_c	convective mass transfer coefficient
k	thermal conductivity
K	permeability
L	cavity width
N	buoyancy ratio, $\left(=\frac{\beta_C \Delta C'}{\beta_T \Delta T}=\frac{\mathrm{Gr}_C}{\mathrm{Gr}_T}\right)$
Nu	Nusselt number
Pe	Peclect number $(=U_o H/\alpha)$
Pr	Prandtl number $(=\nu/\alpha)$
R_i	Richardson number $(=\mathrm{Gr}/\mathrm{Re}^2)$
Re	Reynolds number $(=U_o H/\nu)$
Sc	Schmidt number $(=\nu/D)$
Sh	Sherwood number
t	time
T	temperature
U_o	top wall velocity
U, V	dimensionless interstitial velocity components
u, v	interstitial velocity components
$\mathbf{v}$	interstitial velocity vector
x, y	Cartesian coordinates
X, Y	dimensionless coordinates
α	thermal diffusivity
β_T	thermal expansion coefficient
β_C	solutal expansion coefficient
ε	porosity
θ	dimensionless temperature $[=(T-T_C)/(T_H-T_C)]$
ν	kinematic viscosity
ρ	density
σ	capacity ratio $\{=[\varepsilon(\rho c)_f+(1-\varepsilon)(\rho c)_s]/(\rho c)_f\}$
τ	dimensionless time $(=tU_o/H)$
ψ	stream function
Ψ	dimensionless stream function $(=\psi/HU_o)$
ω	dimensionless vorticity $(=\Omega H/U_o)$
Ω	vorticity

Subscripts

f	fluid
H	hot
L	cold
s	solid

analytically the phenomenon of natural convection caused by combined temperature and concentration buoyancy effects in a rectangular enclosure with uniform heat and mass fluxes applied along the vertical walls.

Double-diffusive natural convection in a fluid-saturated porous medium has received considerable attention in a wide variety of applications such as food processing, geophysical systems, contaminant transport in groundwater, and grain storage. Trevisan and Bejan [9] investigated natural convection with combined heat and mass transfer buoyancy effects in a porous medium subjected to constant temperature and adiabatic wall conditions using Darcy's relation. The numerical results were conducted for a range of Darcy-Rayleigh number, Lewis number, and buoyancy ratio. For many practical engineering applications, Darcy's law is not valid, and boundary and inertial effects need to be accounted for. Chen and Chen [10] considered double-diffusive fingering convection in a porous medium. The Darcy equation including Brinkman and Forchheimer terms to account for viscous and inertia effects was used for the momentum equation. Karimi et al. [11] conducted a numerical analysis of double-diffusive convection in a square cavity filled with a porous medium for various pertinent controlling parameters. Non-Darcian effects were analyzed through investigating the average heat and mass transfer rates. The results of that investigation showed that the inertial and boundary effects have a

significant effect on the double-diffusive convection. Goyeau et al. [12] performed a numerical study on double-diffusive natural convection in a porous cavity using the Darcy-Brinkman formulation. Their numerical results for mass transfer were in excellent agreement with the scaling analysis over a wide range of the controlling parameters, while their heat transfer results showed that the boundary-layer analysis was not a suitable method to predict the correct scales for heat transfer in the same domain. The Darcy model with the Boussinesq approximation was used by Mamou et al. [13] to study soluble-diffusive natural convection in an inclined porous layer subject to transverse gradients of heat and solute. A wide range of controlling parameters was investigated in this study. A good agreement was observed between the analytical predictions and the numerical simulations.

Mixed-convection flow and heat transfer in enclosures has received an impetus in recent years because several applications of practical interest can be found in some industrial processes such as food processing and float glass production [14]. Prasad and Koseff [15] conducted an experimental study of a recirculating mixed-convection flow in a cavity filled with water. For the range of governing parameters studied, their results indicated that the overall heat transfer rate was a very weak function of the Grashof number for the range of Reynolds number examined. The effects of the Prandtl number on laminar mixed-convection heat transfer in a lid-driven cavity were considered numerically by Moallemi and Jang [16]. Their numerical simulations revealed that the influence of the buoyancy on the flow and heat transfer inside cavities was found to be more pronounced for higher values of Prandtl number. Later, Iwatsu et al. [17] studied numerically mixed-convection heat transfer in a driven cavity with a stable vertical temperature gradient. Their results showed that the flow features are similar to those of a conventional driven-cavity of a non-stratified fluid for small values of Richardson number. Also, it was found that when the Richardson number is very high, much of the middle and bottom portions of the cavity interior are stagnant. Recently, Khanafer and Chamkha [18] investigated laminar, mixed-convection flow in an enclosure filled with a Darcian fluid-saturated uniform porous medium in the presence of internal heat generation. Their results showed that the heat transfer mechanisms and the flow characteristics inside the cavity were strongly dependent on the Richardson number. Moreover, the presence of the internal heat-generation effect in the model was found to have significant influence on the features of the isotherms and slight effects on the streamlines for small values of the Richardson number.

Heat and mass transfer in lid-driven enclosures have received less attention in the literature. In drying technology, better understanding of the drying process is vital for optimum performance of the drying chamber [19]. Alleborn et al. [19] investigated a two-dimensional flow accompanied by heat and mass transport in a shallow lid-driven cavity with a moving heated lid and a moving cooled lid. Their results showed that the drying rates were enhanced by increasing the web velocity and become increasingly independent of the gravity orientation because of the dominance of forced convection.

To the best knowledge of the present authors, no attention has been paid to the problem of double-diffusive mixed-convection flow in a lid-driven enclosure filled with a fluid-saturated porous medium. The present study is focused on the analysis of heat and mass transfer in a square enclosure using the generalized model of the

momentum equation. Moreover, a wide range of the pertinent parameters such as the Reynolds number, Richardson number, Lewis number, Buoyancy ratio, and the Darcy number is considered in the present study to show the significance of these parameters on the heat and mass transfer processes.

PROBLEM DEFINITION

Consider a two-dimensional enclosure of height H and width L filled with a fluid-saturated porous medium as shown in Figure 1. The effect of the heat conduction in the solid walls is assumed to be negligible. The vertical walls are assumed to be insulated, nonconducting, and impermeable to mass transfer. The fluid in the enclosure is Newtonian, incompressible, and laminar. The porous medium is assumed to be isotropic, homogeneous, and in thermodynamical equilibrium with the fluid. The effects of Soret (thermal diffusion) and Dufour (diffusion thermo) are neglected in the present study. The top wall, moving at a constant velocity U_o, is kept at high temperature and concentration (T_H and C'_H) while the horizontal wall is kept at low temperature and concentration (T_L and C'_L). The thermophysical properties of the fluid are assumed to be constant except the density variation in the buoyancy force, which is approximated according to the Boussinesq approximation. This variation, due to both temperature and concentration gradients, can be described by the following equation:

$$\rho = \rho_o\left[1 - \beta_T(T - T_L) - \beta_C\left(C' - C'_L\right)\right] \tag{1}$$

where β_T and β_C are the coefficients for thermal and concentration expansions, respectively:

$$\beta_T = -\frac{1}{\rho_o}\left(\frac{\partial\rho}{\partial T}\right)_{P,C} \qquad \beta_C = -\frac{1}{\rho_o}\left(\frac{\partial\rho}{\partial C'}\right)_{P,T} \tag{2}$$

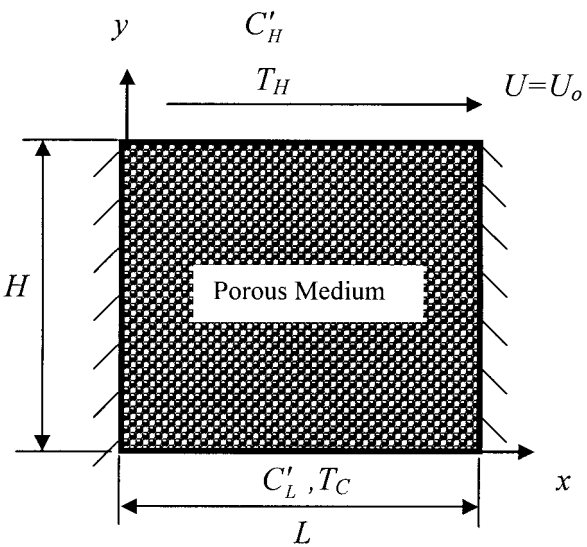

Figure 1. Sketch of the cavity and coordinate system.

In accordance with the problem description, the initial and boundary conditions are presented as

$$u = \mathbf{v} = 0 \qquad T = 0 \qquad C' = 0 \qquad \text{for } t = 0 \tag{3a}$$

$$\left.\begin{array}{lll} u = U_o, \mathbf{v} = 0 & \text{at } y = H & 0 \le x \le L \\ u = \mathbf{v} = 0 & \text{at } y = 0 & 0 \le x \le L \\ u = \mathbf{v} = 0 & \text{at } x = 0, L & 0 \le y \le H \end{array}\right] \quad \text{for } t > 0 \tag{3b}$$

$$\left.\begin{array}{ll} \dfrac{\partial T}{\partial x} = \dfrac{\partial C'}{\partial x} = 0 & \text{at } x = 0, L \quad \text{and} \quad 0 \le y \le H \\ T = T_L, C' = C_L & \text{at } y = 0,\ 0 \le x \le L \\ T = T_H, C' = C_H & \text{at } y = H,\ 0 \le x \le L \end{array}\right\} \quad \text{for } t > 0 \tag{3c}$$

Upon performing transforming the governing equations into the vorticity–stream function formulation, and incorporating the following dimensionless parameters,

$$\left.\begin{array}{llll} \mathrm{X} = \dfrac{x}{H} & Y = \dfrac{y}{H} & \tau = \dfrac{tU_o}{H} & U = \dfrac{u}{U_o} \quad V = \dfrac{\mathbf{v}}{U_o} \\ \omega = \dfrac{\Omega H}{U_o} & \Psi = \dfrac{\psi}{HU_o} & \theta = \dfrac{T - T_L}{T_H - T_L} & C = \dfrac{C' - C'_L}{C'_H - C'_L} \end{array}\right\} \tag{4}$$

we arrive at

$$\varepsilon \frac{\partial \omega}{\partial \tau} + U \frac{\partial \omega}{\partial X} + V \frac{\partial \omega}{\partial Y} = \frac{\varepsilon}{\mathrm{Re}} \left(\frac{\partial^2 \omega}{\partial X^2} + \frac{\partial^2 \omega}{\partial Y^2} \right) - \frac{\varepsilon^2}{\mathrm{Da}\,\mathrm{Re}}\, \omega - \frac{F\varepsilon^2}{\sqrt{\mathrm{Da}}} |\mathbf{v}| \omega + \frac{F\varepsilon^2}{\sqrt{\mathrm{Da}}} \left(U \frac{\partial |\mathbf{v}|}{\partial Y} - V \frac{\partial |\mathbf{v}|}{\partial X} \right) + \frac{\varepsilon^2\, \mathrm{Gr}_T}{\mathrm{Re}^2} \left(\frac{\partial \theta}{\partial X} + N \frac{\partial C}{\partial X} \right) \tag{5}$$

$$\left(\frac{\partial^2 \Psi}{\partial X^2} + \frac{\partial^2 \Psi}{\partial Y^2} \right) = -\omega \tag{6}$$

$$\sigma \frac{\partial \theta}{\partial \tau} + U \frac{\partial \theta}{\partial X} + V \frac{\partial \theta}{\partial Y} = \frac{1}{\mathrm{Re}\,\mathrm{Pr}} \left(\frac{\partial^2 \theta}{\partial X^2} + \frac{\partial^2 \theta}{\partial Y^2} \right) \tag{7}$$

$$\varepsilon \frac{\partial C}{\partial \tau} + U \frac{\partial C}{\partial X} + V \frac{\partial C}{\partial Y} = \frac{1}{\mathrm{Re}\,\mathrm{Sc}} \left(\frac{\partial^2 C}{\partial X^2} + \frac{\partial^2 C}{\partial Y^2} \right) \tag{8}$$

where $\mathrm{Re} = U_o H/\nu$ is the Reynolds number, $\mathrm{Gr}_T = g\beta_T (T_H - T_L) H^3/\nu^2$ is the thermal Grashof number, $\mathrm{Sc} = \nu/D$ is the Schmidt number, $\mathrm{Pr} = \nu/\alpha$ is the Prandtl number, $\sigma = [\varepsilon(\rho c_p)_f + (1-\varepsilon)(\rho c_p)_s]/(\rho c_p)_f$ is the specific heat ratio, $N = (\beta_C \Delta C')/(\beta_T \Delta T) = \mathrm{Gr}_C/\mathrm{Gr}_T$ is the buoyancy ratio, $\mathrm{Gr}_C = g\beta_C (C'_H - C'_L) H^3/\nu^2$ is the solutal Grashof number, $F = \left(1.75\sqrt{U^2 + V^2}\right)/\sqrt{150}\varepsilon^{1.5}$ is the porous

medium inertia coefficient, and $\mathrm{Da} = \kappa/H^2$ is the Darcy number. The aspect ratio of the enclosure is $A = L/H$. The average heat and mass fluxes at the walls are represented in dimensionless forms by the average Nusselt and Sherwood numbers:

$$\mathrm{Nu} = \frac{1}{A}\int_0^A \left(\frac{\partial\theta}{\partial Y}\right)_{Y=0} dX \qquad \text{and} \qquad \mathrm{Sh} = \frac{1}{A}\int_0^A \left(\frac{\partial C}{\partial Y}\right)_{Y=0} dX \tag{9}$$

NUMERICAL METHOD

The governing equations (5)–(8) were descretized using the finite-volume approach [20]. A brief description of the numerical approach is presented here. The governing equations can be represented by a general differential equation as follows:

$$\delta_\phi \frac{\partial\phi}{\partial\tau} + \frac{\partial}{\partial X}\left(U\phi - \Gamma_\phi \frac{\partial\phi}{\partial X}\right) + \frac{\partial}{\partial Y}\left(V\phi - \Gamma_\phi \frac{\partial\phi}{\partial Y}\right) = \bar{S}_\phi \tag{10}$$

where ϕ stands for either ω, θ, or C, with

$$\delta_\phi = \varepsilon \qquad \Gamma_\omega = \frac{\varepsilon}{\mathrm{Re}} \qquad \bar{S}_\omega = \frac{F\varepsilon^2}{\sqrt{\mathrm{Da}}}\left(U\frac{\partial|\mathbf{v}|}{\partial Y} - V\frac{\partial|\mathbf{v}|}{\partial X}\right) - \frac{F\varepsilon^2}{\sqrt{\mathrm{Da}}}|\mathbf{v}|\omega - \frac{\varepsilon^2}{\mathrm{Da}\,\mathrm{Re}}\omega + \varepsilon^2\mathrm{Ri}\left(\frac{\partial\theta}{\partial X} + N\frac{\partial C}{\partial X}\right) \tag{11a}$$

$$\delta_\theta = 1.0 \qquad \Gamma_\theta = \frac{1}{\mathrm{Pe}} \qquad \bar{S}_\theta = 0 \tag{11b}$$

$$\delta_C = \varepsilon \qquad \Gamma_C = \frac{1}{\mathrm{Re}\,\mathrm{Sc}} \qquad \bar{S}_C = 0 \tag{11c}$$

The transient finite-difference equations, Eqs. (5), (7), and (8), were solved using an alternating direct implicit algorithm (ADI) in conjunction with the power-law technique [20]. In addition, a false transient accelerator was implemented to expedite the convergence rate of the solution toward steady-state condition. Furthermore, the successive overrelaxation method (SOR) was applied to solve for the flow kinematics, as described by Eq. (6).

The vorticity on the boundaries is presented from its definition in terms of the primitive velocity variables as

$$\left.\begin{aligned} \omega_{i,1} &= \frac{(-4\,U_{i,2} + U_{i,3})}{2\,\Delta Y} & \omega_{i,N} &= \frac{(-3U_o + 4U_{i,N-1} - U_{i,N-2})}{2\,\Delta Y} \\ \omega_{1,j} &= \frac{(4V_{2,j} - V_{3,j})}{2\,\Delta X} & \omega_{M,j} &= \frac{(-4V_{M-1,j} + V_{M-2,j})}{2\,\Delta X} \end{aligned}\right\} \tag{12}$$

The convergence criteria require that the absolute value of the residual for the vorticity, concentration, and temperature be less than 10^{-6}. To test and assess grid

independence of the solution scheme, many numerical experiments were performed as shown in Figure 2. These experiments showed that an equally spaced grid mesh of 81×81 is adequate to describe the flow and heat and mass transfer processes correctly. Further increase in the number of grid points produced essentially the same results. The validation of the numerical code was performed against the work of Weaver and Viskanta [21] in the absence of porous medium as shown in Figure 3. It can be seen from this figure that the solution of the present numerical code is in excellent agreement with the numerical and experimental results of Weaver and Viskanta [21] for Grashof numbers of $\mathrm{Gr}_T = 5.88 \times 10^5$, 9.31×10^5 and buoyancy ratios of $N = 0.55, -1.85$. Excellent agreement was found between the minimum and maximum values of the stream function of the present results and the numerical results of Weaver and Viskanta [21] as shown in Table 1. Moreover, the present numerical code was also validated against the results of Nithiarasu et al. [22] for double-diffusive natural convection in an enclosure filled with fluid-saturated porous medium for various Biot numbers as shown in Figure 4. It can be seen from the comparison that both solutions are in excellent agreement. Table 2 confirms this agreement between the two solutions. An additional check on the accuracy of the present results was conducted against the results of Karimi et al. [11] for double-diffusive natural convection in a square cavity filled with a porous medium. Table 3 shows a comparison of the variations of the average Nusselt number (or the average Sherwood number) for the generalized model of the momentum equation at various Darcy numbers. Both results were found to be in very good agreement.

DISCUSSION AND RESULTS

The numerical code used in the present investigation has been used to carry out a number of simulations for a wide range of controlling parameters such as buoyancy ratio, Reynolds number, Darcy number, and Lewis number. The range of the buoyancy number N for this investigation was varied in the range $-1{,}500 \leq N \leq 500$. The range of the Reynolds number used in this study was $50 \leq \mathrm{Re} \leq 500$, Darcy number was $10^{-4} \leq \mathrm{Da} \leq 10^{-1}$, and Lewis number was $1 \leq \mathrm{Le} \leq 20$. The other parameters were kept constant: The aspect ratio of the enclosure ($A = 1$), specific heat ratio ($\sigma = 1$), Schmidt number ($\mathrm{Sc} = 1$), thermal Grashof number $\left(\mathrm{Gr}_T = 10^2\right)$, and the porosity of the porous medium was assumed constant ($\varepsilon = 0.95$).

Figure 5 shows the effect of the buoyancy ratio on the streamlines as well as on the isotherms for a wide range of variations in this ratio. It can be seen from Figure 5 that as the buoyancy ratio increases, the mechanical effect of the sliding lid is overwhelmed by the combined effect of the buoyancy forces. Therefore, for very large values of buoyancy ratios, the flow is almost stagnant in the bulk of the interior part of the cavity except at the portions close to the sliding top wall as shown in Figure 5. As the buoyancy ratio increases, for a Lewis number of unity, the effective Richardson number $R_i^* = (1 + N)(\mathrm{Gr}_T/\mathrm{Re}^2)$ increases significantly and, as a result, the temperature stratification is substantially linear in the stagnant bulk of the interior regions. Thus, the overall heat transfer is mostly transferred by conduction in the middle and bottom parts of the enclosure except in a relatively small region close to the top surface, where the induced convective activities are appreciable.

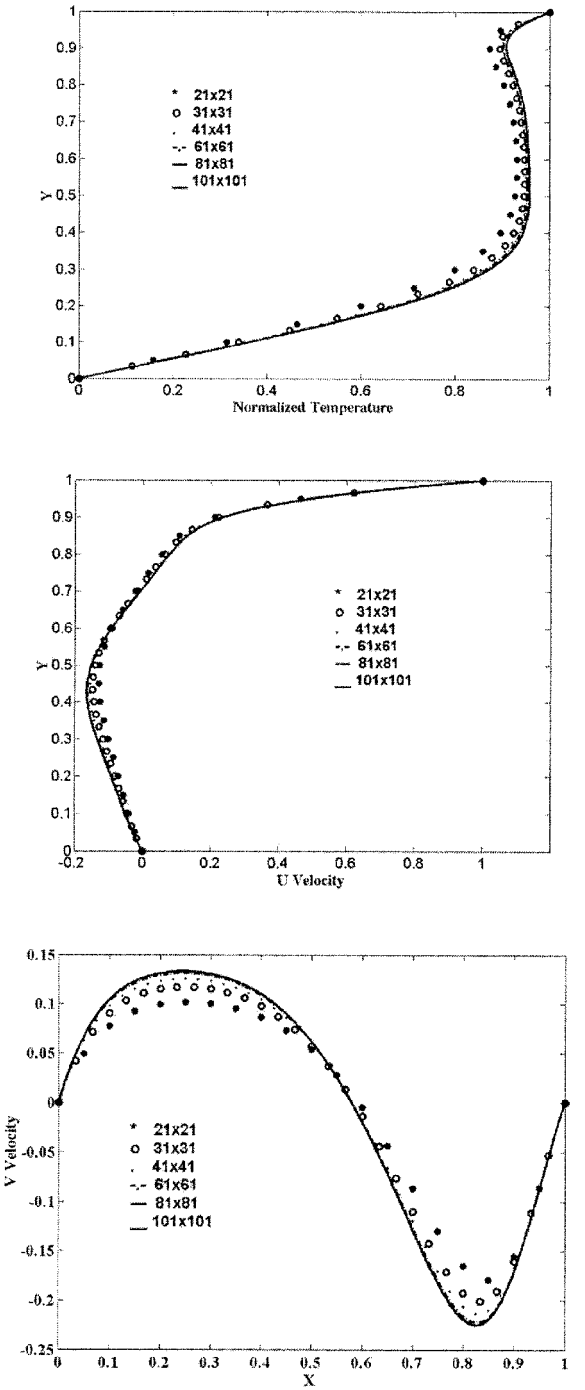

Figure 2. Velocity and temperature profiles at midsections of the cavity for various mesh sizes at $Re = 250$ and $Da = 0.1$.

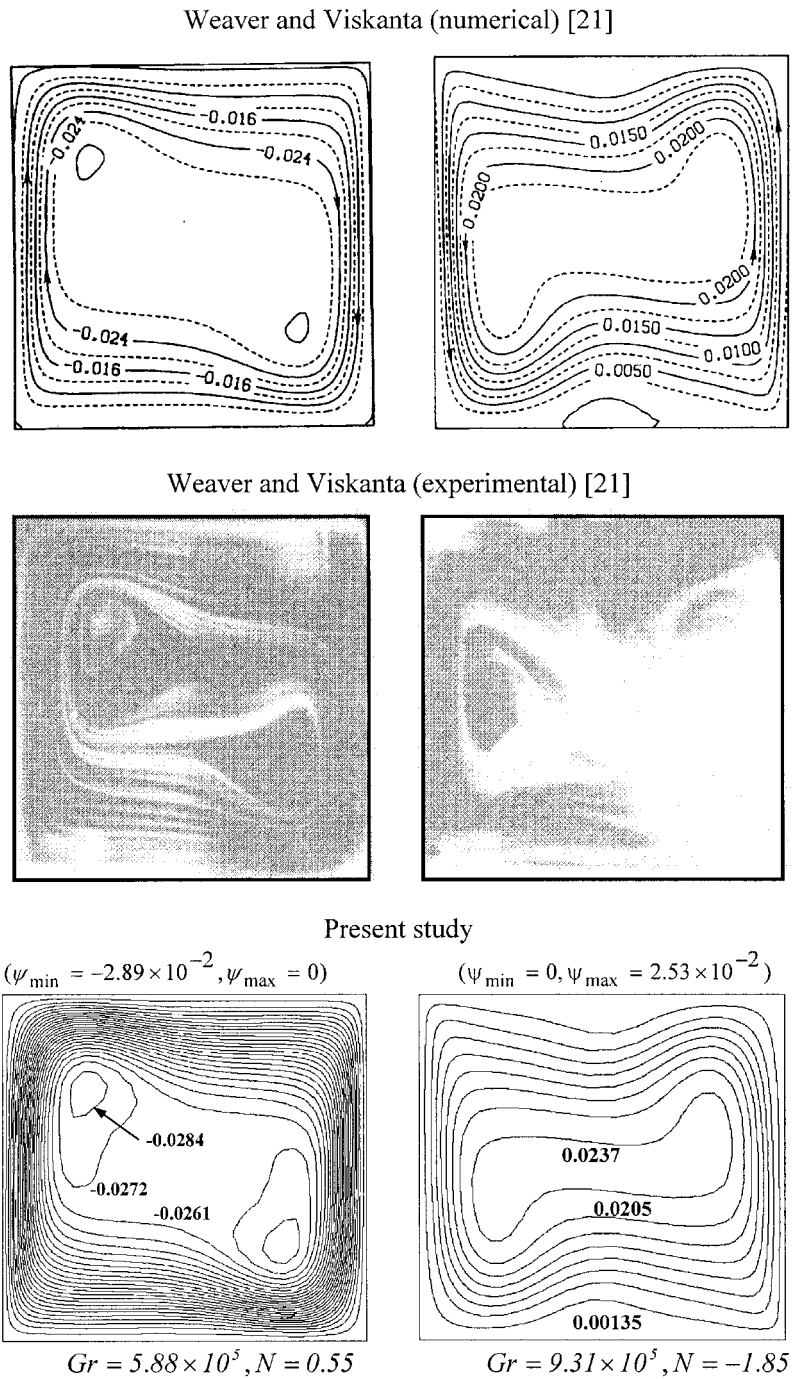

Figure 3. Comparison of streamlines between the present numerical solution and those of Weaver and Viskanta [21].

Table 1. Comparison of minimum and maximum values of the stream function between the present results and those of Weaver and Viskanta [21]

	Present	Weaver and Viskanta [21]	Difference (%)
$(\mathrm{Gr} = 5.88 \times 10^5$ & $N = 0.55)$			
$\Psi_{\min}$	-0.0289	-0.028	3.11
$(\mathrm{Gr} = 9.31 \times 10^5$ & $N = -1.85)$			
$\Psi_{\max}$	0.0253	0.025	1.18

For negative values of the buoyancy ratio ($N < 0$), as shown in Figure 6, the solutal buoyancy is acting in the same direction to the lid-driven wall, which causes the central vortex (vortex with clockwise rotation) to rotate at high velocity. This effect is more pronounced at high buoyancy ratio as a result of predominant influence of the solutal buoyancy. This implies that, due to the vigorous actions of mechanical effect of the lid-driven wall and the effect of the solutal buoyancy, fluids are well mixed and, consequently, the temperature gradients are weak in the bulk of the cavity except for the zones close to the bottom surface, which points to the existence of steep temperature gradients as depicted in Figure 6. This is confirmed in Figure 6, which indicates the variations of the temperature and velocity profiles at the mid-sections of the cavity for various buoyancy ratios. For high negative values of buoyancy ratio, the temperature differences in much of the interior region of the cavity are very small except at zones close to the lid-driven wall and the bottom surface. Moreover, Figure 7 shows that the horizontal velocity is overshooting near the top wall for high negative buoyancy ratio ($N = -1500$), which is caused by the combined effects of the lid-driven wall and the solutal buoyancy. This effect is clearly noticeable with respect to the vertical velocity component along the centerline of the cavity for higher negative values of the buoyancy ratio.

The effect of the variation of Reynolds number on the streamlines and isotherms is shown in Figure 8. It can be seen from this figure that as the Reynolds number increases, the gross flow features are similar to those of a lid-driven enclosure, where the buoyancy effect is overwhelmed by the mechanical effect of the sliding lid. The fluid flow is characterized by a primary recirculating eddy of the size of the enclosure generated by the moving lid and minor eddies near the bottom corners. For small value of Reynolds number, $\mathrm{Re} = 50$, Figure 8 illustrates that the isotherms are nearly parallel to the horizontal wall, indicating that a quasi-conduction region is reached except near the top moving wall, where the mechanical effect of the moving wall is noticeable. For a large value of Reynolds number, $\mathrm{Re} = 500$, the mechanical effect of the top moving wall is dominant and the temperature gradients are very small in most of the interior region of the cavity due to the fact that the fluid is well mixed within the interior region. Moreover, Figure 8 shows that as the Reynolds number increases, the thermal boundary layer is thinner near the bottom surface, which indicates steep temperature gradients in the vertical direction.

The effect of the presence of the porous medium on the streamlines and isotherms is shown in Figure 9 for various Darcy numbers. Consider a case of equal thermal and solutal Grashof numbers ($\mathrm{Gr}_T = \mathrm{Gr}_C = 10^2$) and Lewis number of unity. It can be seen from this figure that as the Darcy number decreases, the

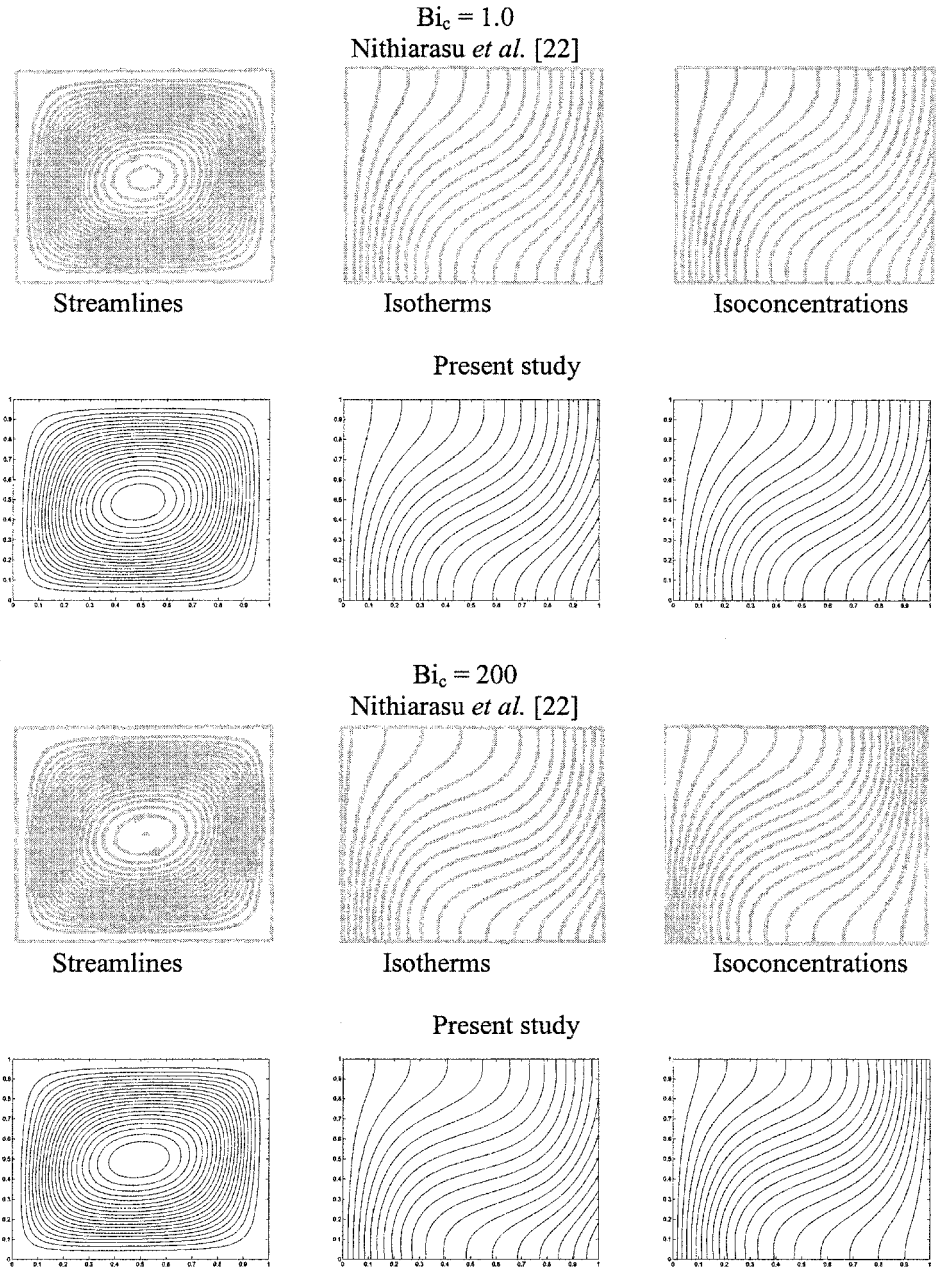

Figure 4. Comparison of streamlines, isotherms, and isoconcentrations between the present numerical results and those of Nithiarasu et al. [22] for different Biot numbers.

microscopic drag force increases, which suppresses the buoyancy forces and consequently decreases the heat and mass transfer rates. Figure 9 shows that as the Darcy number decreases, the dynamic boundary layers are thinner close to the top moving

Table 2. Comparison of maximum values of the stream function and minimum values of temperature and concentration between the present results and those of Nithiarasu et al. [22]

	Present	Nithiarasu et al. [22]	Difference (%)
($Da = 10^{-2}$, $Ra = 10^4$, $\varepsilon = 0.6$, $Bi_T = 1$, $Pr = Sc = 1$ and $N = 1$)			
($Bi_C = 1.0$)			
$\lvert\Psi_{max}\rvert$	2.041	2.042	0.049
T_{min}	0.5089	0.504	0.96
c_{min}	0.5089	0.504	0.96
($Bi_C = 200$)			
$\lvert\Psi_{max}\rvert$	2.846	2.854	0.281
T_{min}	0.5412	0.538	0.59
c_{min}	0.0021	0.002	4.76

Table 3. Comparison of average Nusselt number (or average Sherwood number) between the present results and those of Karimi et al. [11] ($Pr = Sc = 1$ and $Gr_T = Gr_C = 10^5$)

Da	Present Nu (or Sh)	Karimi et al. [11] Nu (or Sh)	Difference (%)
10^{-2}	5.43	5.45	0.36
10^{-3}	3.54	3.63	2.54
10^{-4}	1.24	1.26	1.6

wall, resulting in high fluid flow velocity in the horizontal direction and consequently high viscous forces near the top moving wall. For very small values of Darcy numbers, the fluid experiences a pronounced large resistance as it flows through the porous matrix, causing the flow to cease in the bulk of the cavity. In this situation, the convective heat transfer mechanism is almost suppressed and the isotherms are almost parallel to the horizontal wall, indicating a pure-conduction regime in the bulk of the enclosure except near the top wall, where the effect of the lid-driven wall is significant.

The effect of the buoyancy ratio on the streamlines, isotherms, and iso-concentration contours for high Lewis number is shown in Figure 10. It can be seen from this figure that the isotherms are almost parallel to the horizontal wall for all values of the buoyancy ratios, indicating that most of the heat transfer is carried out by heat conduction. This due to an increase in the thermal boundary-layer thickness as the Lewis number increases. Moreover, Figure 10 clearly shows that the iso-concentration contours are enhanced for high Lewis number and small values of buoyancy ratio. As mentioned before, as the Lewis number increases, the solutal boundary-layer thickness decreases and consequently enhances thermosolutal activities in the enclosure. As the buoyancy ratio increases for high Lewis number, mass transfer is inhibited as shown in Figure 10 except at the top wall, where the mechanical effect of the lid-driven wall is significant. At low buoyancy ratio, the entire enclosure is influenced by the flow structure and as the buoyancy ratio increases the boundary-layer thickness becomes thinner. This change in the flow structure for high buoyancy ratio has a significant influence on the concentration

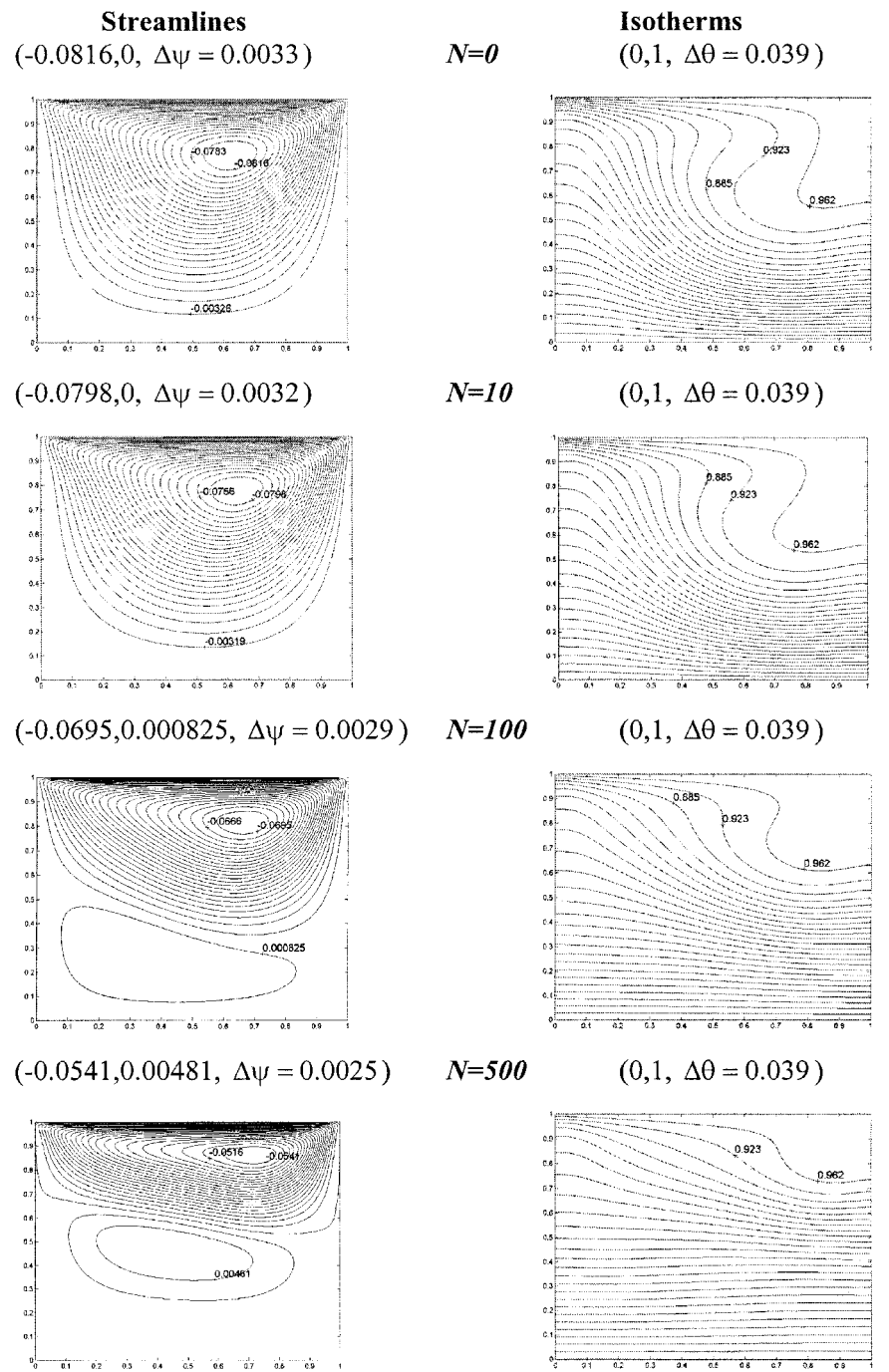

Figure 5. Effect of positive buoyancy ratio values on the streamlines and isotherms for $Re = 100$, $Le = 1$, and $Da = 0.1$.

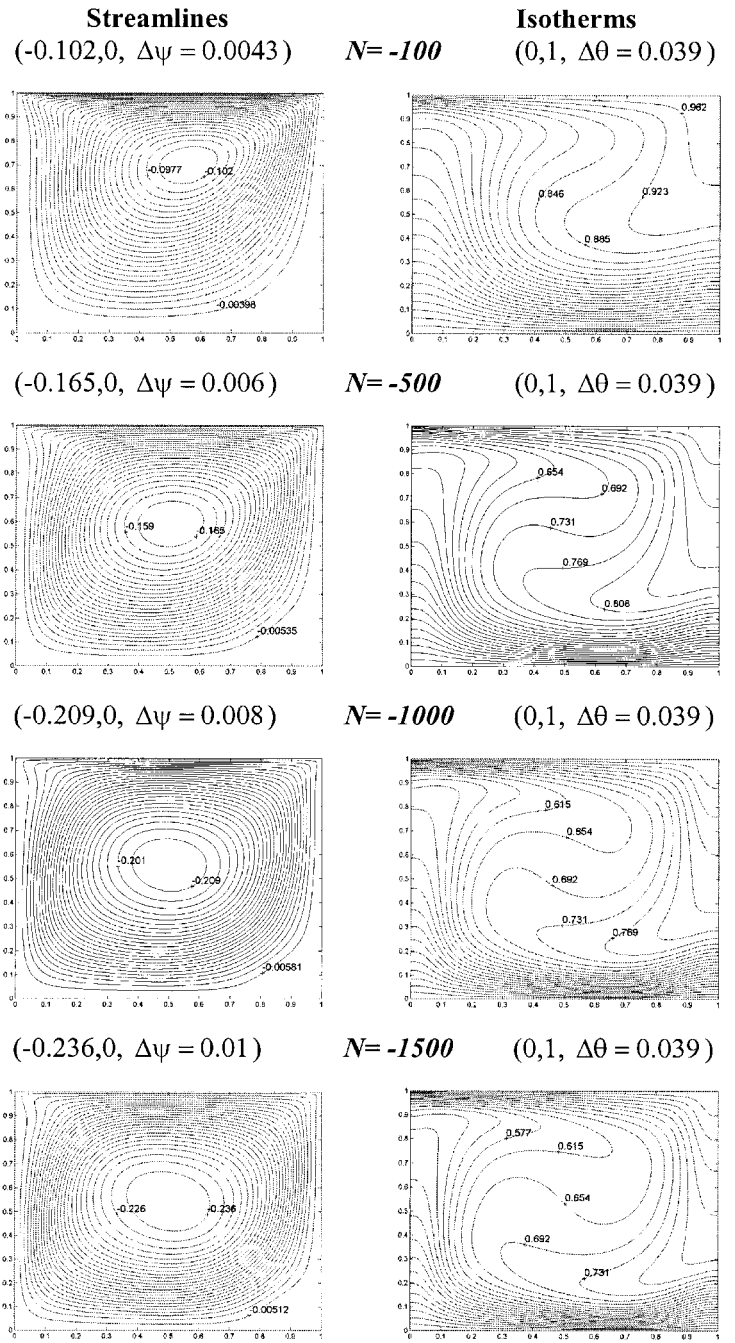

Figure 6. Effect of negative buoyancy ratio values on the streamlines and isotherms for Re = 100, Le = 1, and Da = 0.1.

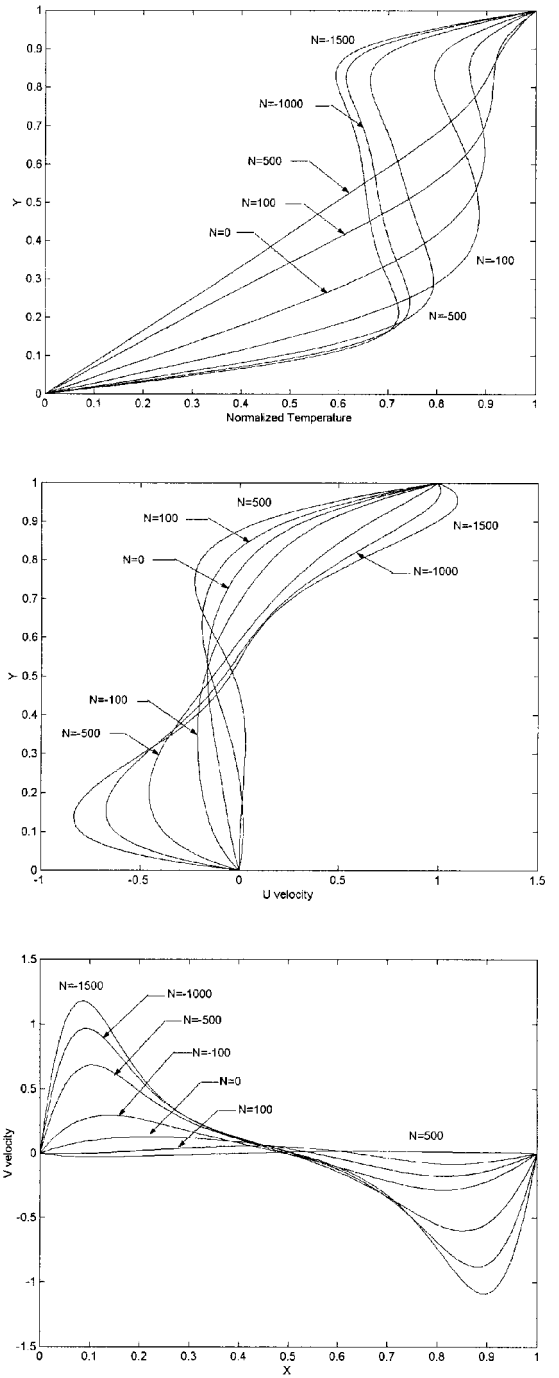

Figure 7. Effect of buoyancy ratio on the temperature and velocity profiles at midsections of the cavity for $Re = 100$, $Le = 1$, and $Da = 0.1$.

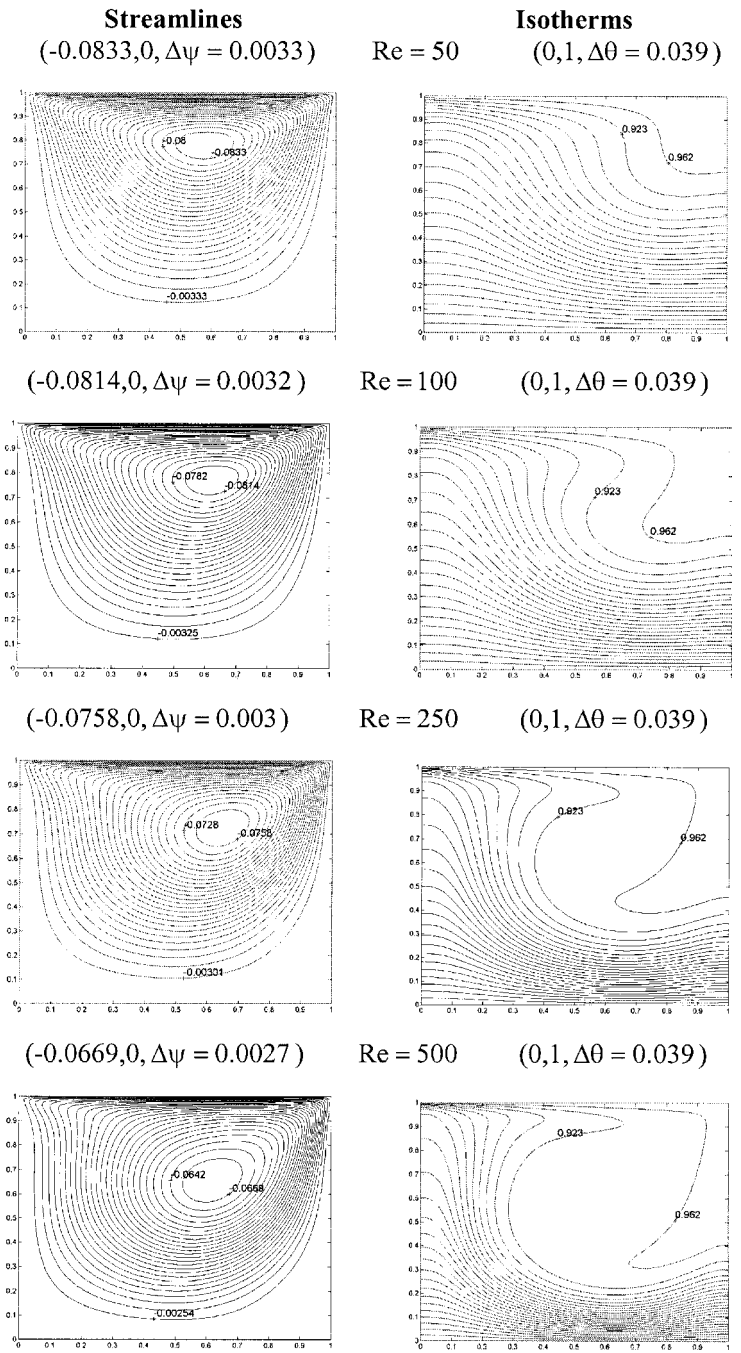

Figure 8. Effect of Reynolds number on the streamlines and isotherms for Le = 1, Da = 0.1, and Grashof number $Gr_T = 10^2$.

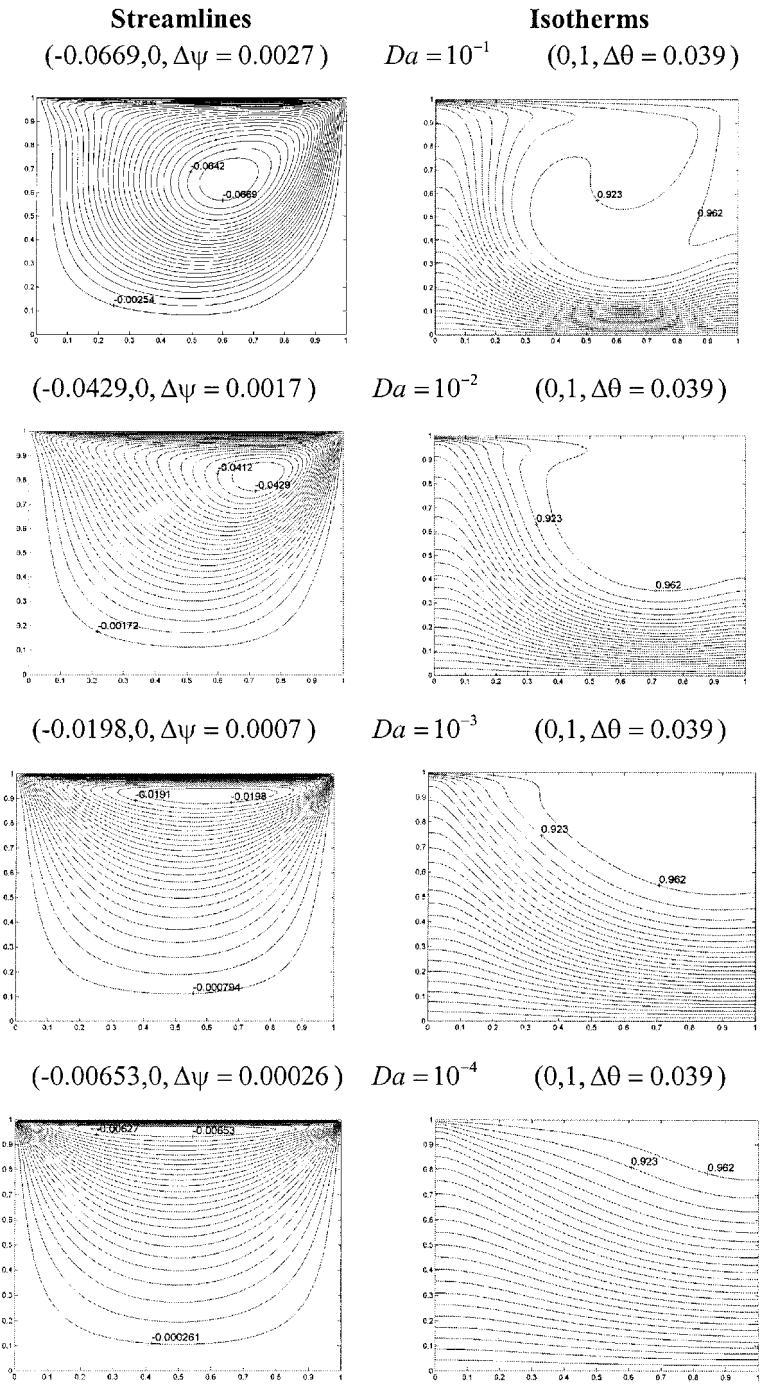

Figure 9. Effect of Darcy number on the streamlines and the isotherms contours for Le = 1.0 and Re = 500.

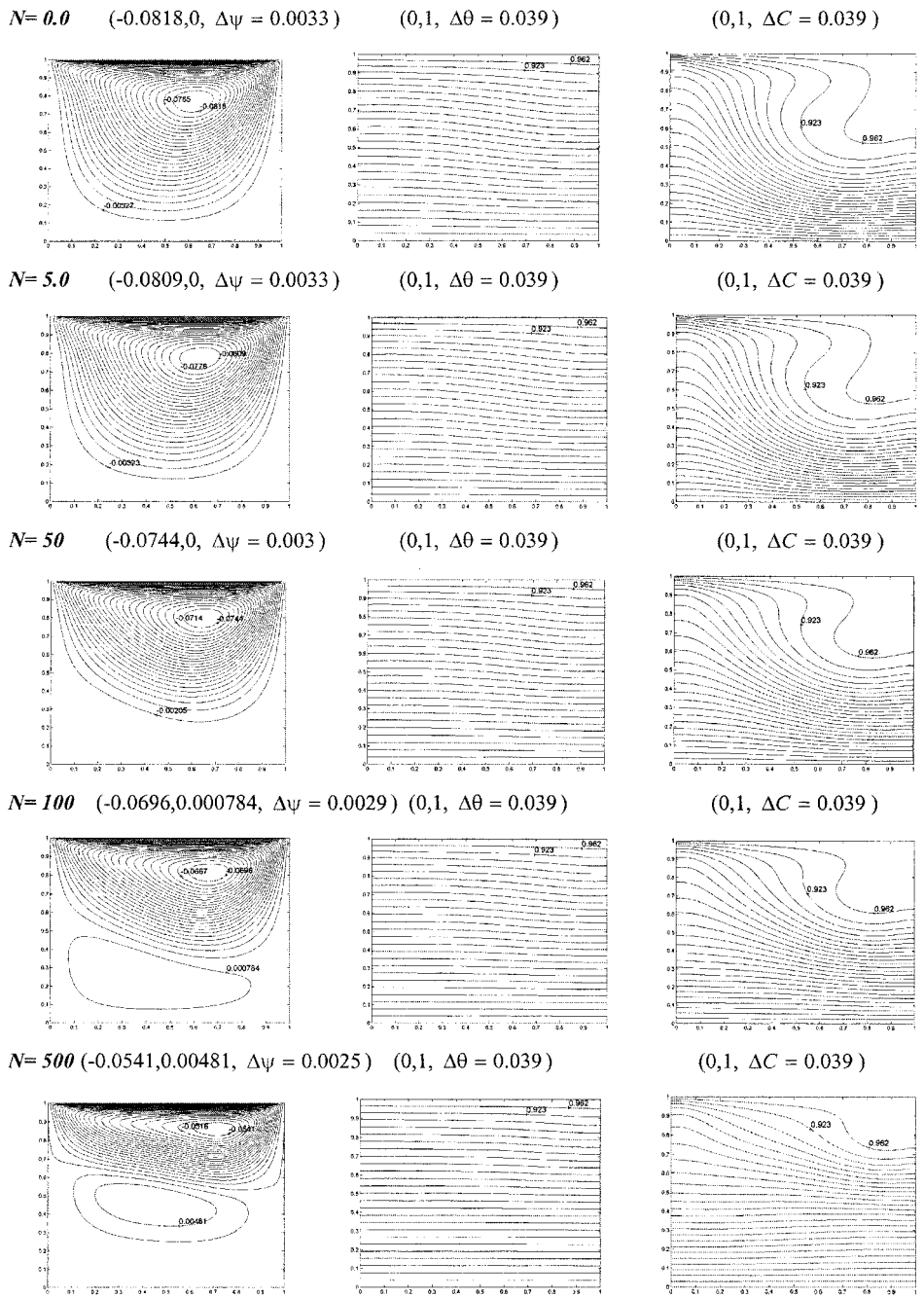

Figure 10. Effect of buoyancy ratio on the streamlines, isotherms, and isoconcentrations for various buoyancy ratios and $\mathrm{Re} = 100$, $\mathrm{Le} = 20$, and $\mathrm{Da} = 10^{-1}$.

field, which increasingly builds up a vertical stratification except near the top wall of the enclosure. This vertical stratification corresponds to minimum heat and mass transfer rates.

The effect of the Darcy number on the streamlines, isotherms, and isoconcentration contours for a high Lewis number (Le = 10) and a Richardson number of ($R_i = \mathrm{Gr}_T/\mathrm{Re}^2 = 4 \times 10^{-4}$) is shown in Figure 11. It is seen that as the Lewis number increases (Le = 10), the isotherm distribution is conduction dominated except near the top surface. Moreover, the Richardson number provides a measure of the importance of the thermal natural convection relative to the lid-driven forced convection. For very small values of Richardson number, the buoyancy effect is overwhelmed by the lid-driven top wall, resulting in a vertical stratification inside the enclosure. The effect of Darcy number on the isoconcentration contours is illustrated in Figure 11. This effect is more pronounced at

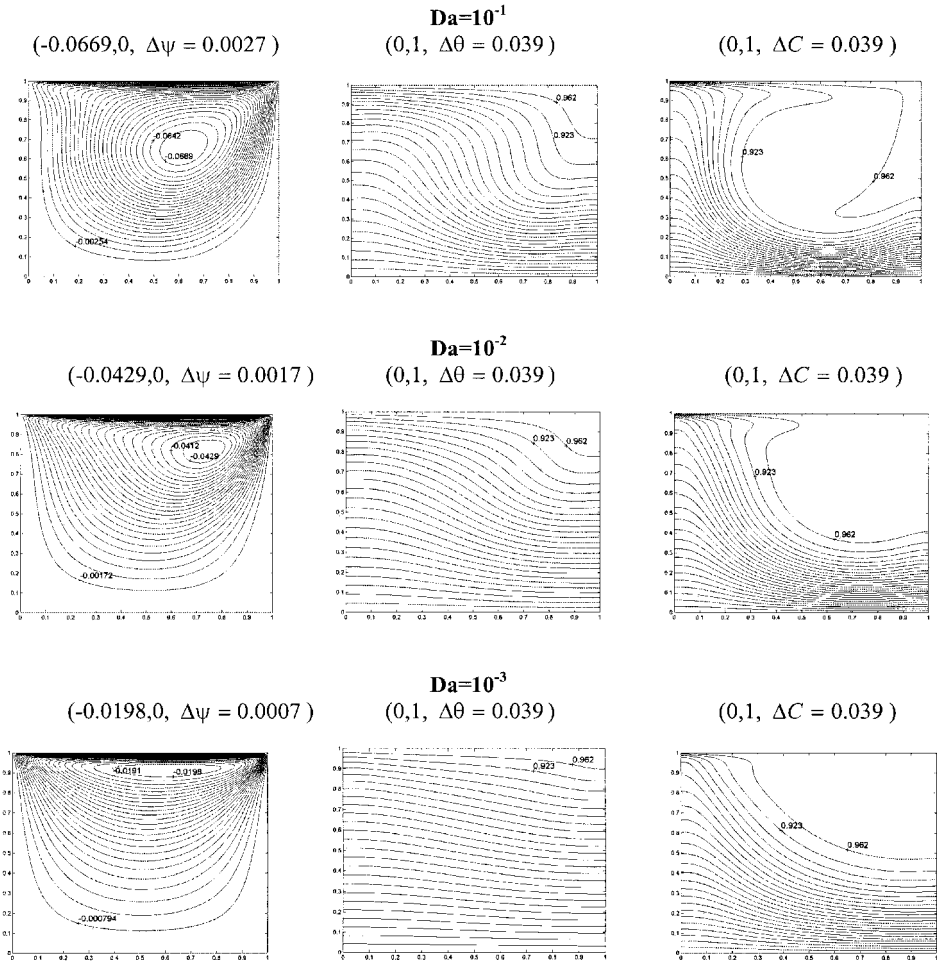

Figure 11. Effect of Darcy number on the streamlines, isotherms, and isoconcentrations for Re = 500, Pr = 0.1, Sc = 1.0, and $\mathrm{Gr}_T = \mathrm{Gr}_C = 10^2$.

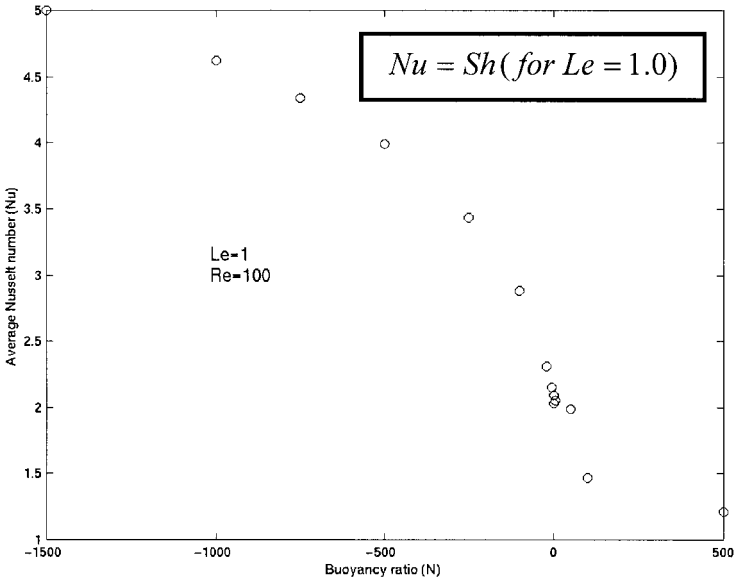

Figure 12. Effect of buoyancy ratio on the average Nusselt number (or average Sherwood number) for $Le = 1$ and $Re = 100$.

very small values of the Darcy number, where the isoconcentration contours are parallel to the horizontal surface except near the top surface. This can be attributed to the lid-driven forced convection and the relatively high Lewis number. For high Lewis numbers, the solutal boundary-layer thickness decreases, resulting in higher concentration rates.

Finally, the effect of the buoyancy ratio on the average Nusselt number (or average Sherwood number) at the bottom surface of the enclosure is shown in Figure 12. This figure shows that as the buoyancy ratio increases, the average Nusselt number (or the Sherwood number) decreases and approaches unity for higher positive values of the buoyancy ratio. However, for negative values of the buoyancy ratio, the average Nusselt number (or average Sherwood number) increases significantly for higher negative values of the buoyancy ratios. This can be attributed to the combined effect of the moving wall and the solutal buoyancy force, which enhances the thermal activity within the enclosure.

CONCLUSIONS

Double-diffusive mixed convection in a square enclosure filled with a porous medium in the presence of moving boundary was formulated and solved numerically. The finite-volume approach was employed along with the alternating direction implicit scheme for the present investigation. The influence of the buoyancy ratio, Lewis number, Reynolds number, and Darcy number on heat and mass transfer processes was analyzed. The results showed that the heat transfer mechanism and the flow characteristics inside the cavity are strongly dependent on the Richardson

number. The results also illustrated significant suppression of the convective currents for higher values of the Lewis number in the presence of a porous medium. Moreover, the results showed noticeable enhancement in the thermal activities inside the enclosure for higher negative values of the buoyancy ratio.

REFERENCES

1. J. P. Coulter and S. I. Guceri, Laminar and Turbulent Natural Convection in Solar Energy Applications, in *Solar Energy Utilization, Proc. NATO Advanced Study Institute*, pp. 303–333, Martinus Nijhoff, Dordrecht, The Netherlands, 1987.
2. T. Nishimura, T. Imoto, and H. Miyashita, Occurrence and Development of Double-Diffusive Convection During Solidification of a Binary System, *Int. J. Heat Mass Transfer*, vol. 37, pp. 1455–1464, 1994.
3. B. I. Makham and F. Rosenberger, Diffusive Convection Vapor Transport Across Horizontal and Inclined Rectangular Enclosures, *J. Crystal Growth*, vol. 67, pp. 241–254, 1984.
4. T. L. Bergman, F. P. Incropera, and R. Viskanta, Correlation of Mixed Layer Growth in a Double-Diffusive, Salt-Stratified System Heated from Below, *J. Heat Transfer*, vol. 108, pp. 206–211, 1986.
5. J.-O. Carlsson, Processes in Interfacial Zones During Chemical Vapor Deposition: Aspects of Kinetics, Mechanisms, Adhesion and Substrate Atom Transport, *Thin Solid Films*, vol. 130, pp. 261–282, 1985.
6. S. Ostrach, Natural Convection with Combined Driving Forces, *PhysicoChem. Hydrodynam.*, vol. 1, pp. 233–247, 1980.
7. P. Ranganathan and R. Viskanta, Natural Convection in a Square Cavity Due to Combined Driving Forces, *Numer. Heat Transfer*, vol. 14, pp. 35–59, 1988.
8. O. V. Trevisan and A. Bejan, Combined Heat and Mass Transfer by Natural Convection in a Vertical Enclosure, *J. Heat Transfer*, vol. 109, pp. 104–112, 1987.
9. O. V. Trevisan and A. Bejan, Natural Convection with Combined Heat and Mass Transfer Buoyancy Effects in a Porous Medium, *Int. J. Heat Mass Transfer*, vol. 28, pp. 1597–1611, 1985.
10. F. Chen and C. F. Chen, Double-Diffusive Fingering Convection in a Porous Medium, *Int. J. Heat Mass Transfer*, vol. 36, pp. 793–807, 1993.
11. M. Karimi-Fard, M. C. Charrier-Mojtabi, and K. Vafai, Non-Darcian Effects on Double-Diffusive Convection Within a Porous Medium, *Numer. Heat Transfer A*, vol. 31, pp. 837–852, 1997.
12. B. Goyeau, J.-P. Songbe, and D. Gobin, Numerical Study of Double-Diffusive Natural Convection in a Porous Cavity Using the Darcy-Brinkman Formulation, *Int. J. Heat Mass Transfer*, vol. 39, pp. 1363–1378, 1996.
13. M. Mamou, P. Vasseur, E. Bilgen, and D. Gobin, Double-Diffusive Convection in an Inclined Slot Filled with Porous Medium, *Eur. J. Mech. B/Fluids*, vol. 14, pp. 629–652, 1995.
14. L. A. B. Pilkington, Review Lecture: The Float Glass Process, *Proc. R. Soc. Lnd. IA*, vol. 314, pp. 1–25, 1969.
15. A. K. Prasad and J. R. Koseff, Combined Forced and Natural Convection Heat Transfer in a Deep Lid-Driven Cavity Flow, in *Heat Transfer in Convective Flows*, HTD-107, pp. 155–162 ASME, New York, 1989.
16. M. K. Moallemi and K. S. Jang, Prandtl Number Effects on Laminar Mixed Convection Heat Transfer in a Lid-Driven Cavity, *Int. J. Heat Mass Transfer*, vol. 35, pp. 1881–1892, 1992.

17. R. Iwatsu, J. M. Hyun, and K. Kuwahara, Mixed Convection in a Driven Cavity with a Stable Vertical Temperature Gradient, *Int. J. Heat Mass Transfer*, vol. 36, pp. 1601–1608, 1993.
18. K. Khanafer and A. J. Chamkha, Mixed Convection Flow in a Lid-Driven Enclosure Filled with a Fluid-Saturated Porous Medium, *Int. J. Heat Mass Transfer*, vol. 42, pp. 2465–2481, 1998.
19. N. Alleborn, H. Raszillier, and F. Durst, Lid-Driven Cavity with Heat and Mass Transport, *Int. J. Heat Mass Transfer*, vol. 42, pp. 833–853, 1999.
20. S. V. Patankar, *Numerical Heat Transfer and Fluid Flow*, Hemisphere, Washington, DC, 1980.
21. J. A. Weaver and R. Viskanta, Natural Convection in Binary Gases Due to Horizontal Thermal and Solutal Gradients, *J. Heat Transfer*, vol. 113, pp. 141–147, 1991.
22. P. Nithiarasu, K. N. Seetharamu, and T. Sundarajan, Double-Diffusive Natural Convection in an Enclosure Filled with Fluid-Saturated Porous Medium: A Generalized Non-Darcy Approach, *Numer. Heat Transfer A*, vol. 30, pp. 413–426, 1996.